

# A unified framework for integrating soundproof and compressible equations of all-scale atmospheric dynamics

Piotr K. Smolarkiewicz, Christian Kühnlein, Nils P. Wedi

*European Centre for Medium-Range Weather Forecasts  
Reading, RG2 9AX, UK  
smolar@ecmwf.int*

## ABSTRACT

The paper describes a numerical framework for consistent integrations of soundproof and compressible nonhydrostatic equations of motion for all-scale atmospheric flows. The development extends a proven numerical model for integrating soundproof equations to fully compressible Euler equations. The unified approach relies on non-oscillatory forward-in-time transport methods, applied consistently to all dependent variables of the system at hand, with implicit representation of buoyant and rotational modes of motion. When the fully compressible equations are solved, the framework allows for either an explicit or implicit representation of acoustic modes. The differences between the large-time-step soundproof and compressible integrators reduce in essence to selection of either a prescribed or a numerically prognosed density, and extension of the Poisson solver to a Helmholtz solver. The numerical advancements and the relative merits of soundproof and compressible PDEs are illustrated at hydrostatic and nonhydrostatic resolutions with, respectively, canonical simulations of planetary baroclinic instability and breaking of deep stratospheric gravity waves.

## 1 Introduction

Hydrostatic balance is fundamental to the maintenance of the Earth's atmosphere, and on average the Earth's atmosphere is always close to hydrostatic equilibrium. This fact has been used to approximate the Euler equations underlying global NWP models, and the resulting approximated hydrostatic primitive equations (HPEs) have been successfully applied in weather and climate prediction for the past 30 years. However, with the rapid progress of high-performance computing, numerical models for simulating general atmospheric circulation can already achieve spatial resolutions outside the domain of validity of HPEs. While the capability to capture nonhydrostatic effects and directly simulate convective motions opens new avenues for all-scale simulations of atmospheric circulations [52], it also puts new demands on the mathematical/physical theories and on the numerical methods used. For example, the simulated vertical extent of the atmosphere is relatively thin compared to its horizontal extent, and vertically propagating sound waves admitted by the fully compressible Euler equations impose severe restrictions on the numerical algorithms used. HPEs are advantageous in this respect as they filter vertically propagating sound waves by virtue of the hydrostatic approximation, thus permitting large time-steps in the numerical integration. Moreover, HPEs imply the separability of horizontal and vertical discretisation, thus facilitating the design of effective semi-implicit flow solvers. Both aspects have been central to the development and the success of weather and climate prediction.

The imperative to drop the hydrostatic approximation with increasing resolution has opened a debate on the theoretical formulation optimal for NWP and climate models. Compressible dynamics are universally valid for atmospheric motions (that is, high Reynolds number, low Mach number flows) across the range of scales from cloud micro-turbulence to planetary circulations. On the other hand, they admit acoustic modes — arguably of relatively little physical significance due to their low energy compared to other modes of motion — that provide serious computational drawbacks due to the large and vari-

able speed of sound in the stratified terrestrial atmosphere [17]. Notwithstanding, most efforts in NWP have been directed so far into solving the fully compressible equations, dismissing soundproof systems as unsuitable for modelling weather and climate based on scale or linear analysis; cf. [9] and references therein. Historically however, the majority of research in low Mach number flows under gravity, ranging from planetary atmospheres and oceans to mantle and solar convection, has relied on reduced soundproof equations that retain thermal aspects of compressibility but are free of acoustic modes. In particular, there is a body of literature attesting to the efficiency, accuracy and versatility of (large-time-step) soundproof models for a wide-ranging array of physical applications [43]. Accordingly, there is an interest to utilise the virtues of sound-proof concepts in global nonhydrostatic NWP and climate models.

This paper describes a unified numerical framework augmenting an established soundproof model [28] with consistent integrators of a suite of all-scale nonhydrostatic PDEs, namely: the anelastic [22, 23], the pseudo-incompressible [11], the Euler equations of gas dynamics [42], and the newly derived large-time-step semi-implicit solvers for the compressible Euler equations of weather and climate [47]. For simplicity and conciseness, and to keep the paper focused on the relative merits of soundproof and fully compressible solvers, the presentation is focused on the formulation of the model dynamical core; i.e., restricted to inviscid, adiabatic dry motions. For the numerical experimentation on large scales, an idealised problem of planetary baroclinic instability [43] is adapted after [14]. For the simulation of nonhydrostatic scales of motion we select the idealisation of a non-Boussinesq amplification and breaking of deep stratospheric mountain waves, following calculations in [44]. These two problems epitomise the transient evolution of planetary Rossby waves and mesoscale gravity wave dynamics.

The paper is organised as follows. In the following section we first introduce the three sets of nonhydrostatic governing equations, combined into a single physically intuitive Cartesian vector form, in abstraction from the model geometry and the coordinate frame adopted. Then we recast this generalized set of PDEs in a form consistent with the problem geometry and the unified solution procedure. The thrust of the paper is in section 3, where we present the common numerical algorithm for integrating the generalised set of the governing PDEs put forward in section 2. In section 4 we demonstrate the efficacy of this unified numerical framework in the comparison of soundproof and compressible solutions to the two idealised problems relevant to weather and climate. Section 5 concludes the paper.

## 2 Governing equations

### 2.1 Generalised governing PDEs; evolutionary Cartesian form

It is practical to view the three nonhydrostatic systems addressed in this paper — the anelastic equations of Lipps and Hemler [22, 23], the pseudoincompressible equations of Durran [11] and the fully compressible Euler equations — as special cases of a single generalised equation set. We consider first a physically intuitive, evolutionary form of the governing equations posed in a rotating Cartesian reference frame, so the generalised system can be compactly written as follows:

$$\frac{d\mathbf{u}}{dt} = -\Theta\nabla\varphi - \mathbf{g}\Upsilon_B \frac{\theta'}{\theta_b} - \mathbf{f} \times (\mathbf{u} - \Upsilon_C \mathbf{u}_e) , \quad (1)$$

$$\frac{d\theta'}{dt} = -\mathbf{u} \cdot \nabla\theta_e , \quad (2)$$

$$\frac{d\varrho}{dt} = -\varrho\nabla \cdot \mathbf{u} . \quad (3)$$

In (1)-(3) the generalised density and pressure variables  $\varrho$  and  $\varphi$  for, respectively, the [anelastic, pseudo-incompressible, compressible] PDE sets are defined as

$$\varrho := [\rho_b(z), \rho_b \frac{\theta_b(z)}{\theta_0}, \rho(\mathbf{x}, t)] , \quad (4)$$

$$\varphi := [c_p \theta_b \pi', c_p \theta_0 \pi', c_p \theta_0 \pi'] , \quad (5)$$

together with corresponding dimensionless coefficients

$$\begin{aligned} \Theta &:= \left[ 1, \frac{\theta(\mathbf{x}, t)}{\theta_0}, \frac{\theta(\mathbf{x}, t)}{\theta_0} \right] , \\ \Upsilon_B &:= \left[ 1, \frac{\theta_b(z)}{\theta_e(\mathbf{x})}, \frac{\theta_b(z)}{\theta_e(\mathbf{x})} \right] , \\ \Upsilon_C &:= \left[ 1, \frac{\theta(\mathbf{x}, t)}{\theta_e(\mathbf{x})}, \frac{\theta(\mathbf{x}, t)}{\theta_e(\mathbf{x})} \right] . \end{aligned} \quad (6)$$

Here:  $\rho$  refers to density;  $\pi \equiv (p/p_0)^{R_d/c_p}$  denotes the Exner-function of pressure, where  $R_d$  and  $c_p$  are the gas constant for dry air and the specific heat at constant pressure, and  $p_0$  is a constant reference pressure;  $\theta$  refers to potential temperature with  $\theta_0$  denoting a constant reference value. Furthermore, subscript “ $b$ ” indicates the basic (reference) hydrostatically balanced state defined here by constant stratification  $S = d \ln \theta_b / dz = N^2 / g \geq 0$ , with  $N$  and  $g$  representing, respectively, the Brunt-Väisälä (buoyancy) frequency and the magnitude of the gravitational acceleration  $\mathbf{g} = (0, 0, -g)$ ; cf. [7]. Primes appearing by the Exner function in (5) denote perturbation with respect to an ambient value  $\pi_e$  that together with ambient velocity,  $\mathbf{u}_e$ , and potential temperature,  $\theta_e$ , defines an auxiliary ambient state  $(\mathbf{u}_e, \phi_e, \theta_e)$  assumed to be a known particular solution of each subset of PDEs comprising the generalised system described below. The primary role of ambient states is to simplify the design of the initial and boundary conditions as well as to enhance the accuracy of calculations in finite-precision arithmetics. Although ambient states can be generally time-dependent (e.g., prescribing oceanic tidal motions [49]), here only stationary ambient states are considered (e.g., geostrophically and thermally balanced large-scale flows [37, 41, 13]). While the basic state can be the same for all three sets of the addressed PDEs, the ambient states generally are not, because they are derived as a compatibility condition from the governing equations. To illustrate, the geostrophic balance for the anelastic versus pseudo-incompressible and compressible Euler equations satisfy, respectively,

$$0 = -\nabla(c_p \theta_b (\pi_e - \pi_b)) - \mathbf{g} \frac{\theta_e - \theta_b}{\theta_b} - \mathbf{f} \times \mathbf{u}_e , \quad (7)$$

$$0 = -c_p \theta_e \nabla(\pi_e - \pi_b) - \mathbf{g} \frac{\theta_e - \theta_b}{\theta_b} - \mathbf{f} \times \mathbf{u}_e , \quad (8)$$

and  $\mathbf{f} \equiv 2\mathbf{\Omega}$ , where  $\mathbf{\Omega}$  marks the Earth’s angular velocity.

At a glance (1)-(3) take a form of compressible equations, which can be misleading if taken out of context. The proper interpretation of this system depends on the definition of the generalised density used in (3): either as a prescribed problem parameter for the anelastic and pseudo-incompressible systems according to the specifications in (4), or as a dependent prognostic variable with the associated constitutive law

$$\varphi = c_p \theta_0 \left[ \left( \frac{R_d}{p_0} \varrho \theta \right)^{R_d/c_v} - \pi_e \right] . \quad (9)$$

Noteworthy, the anelastic and the pseudo-incompressible equations, do not necessitate the provision of constitutive laws for their solution, because their respective pressure perturbations are determined from the elliptic equations that follow from constraining the velocity solutions to satisfy mass continuity equation

$$\nabla \cdot (\varrho \mathbf{u}) = 0 , \quad (10)$$

to which (9) reduces for prescribed soundproof densities in (4). In other words, their constitutive laws were analytically accounted for while deriving the reduced equations, and afterwards are not required unless there is a need to provide, say, temperature perturbations for moist thermodynamics. This is not the case with fully compressible equations where the ideal gas law in (9) explicitly relates the thermodynamic pressure perturbations to the distribution of entropy and mass in the fluid.

## 2.2 Conservative formulation

The evolutionary equations (1)-(3) can be further manipulated to generate abstract forms useful for designing conservative numerical integrators. For example, combining  $\varrho \cdot (1)$  with  $\mathbf{u} \cdot (3)$ , and  $\varrho \cdot (2)$  with  $\theta' \cdot (3)$ , and combining the rhs of (3) with the total derivative  $d\varrho/dt$  on the left-hand-side (lhs), leads to the set of conservation laws

$$\frac{\partial \varrho \mathbf{u}}{\partial t} + \nabla \cdot (\varrho \mathbf{u} \otimes \mathbf{u}) = \varrho \mathbf{R}^{\mathbf{u}}, \quad (11)$$

$$\frac{\partial \varrho \theta'}{\partial t} + \nabla \cdot (\varrho \theta') = \varrho R^{\theta}, \quad (12)$$

$$\frac{\partial \varrho}{\partial t} + \nabla \cdot (\varrho \mathbf{u}) = 0, \quad (13)$$

wherein  $\mathbf{R}^{\mathbf{u}}$  and  $R^{\theta}$  symbolise right-hand-sides of (1) and (2), respectively, and  $\otimes$  denotes the tensor product. The prognostic momentum (1) and entropy (2) equations can be viewed as the generic Lagrangian form

$$\frac{d\psi}{dt} = R, \quad (14)$$

whereas (11) and (12) can be viewed as the generic conservation law

$$\frac{\partial \varrho \psi}{\partial t} + \nabla \cdot (\varrho \mathbf{u} \psi) = \varrho R, \quad (15)$$

with  $\psi$  symbolising the three components of the velocity vector and potential temperature perturbation, while  $R$  denotes the associated right-hand-sides.

## 2.3 Extension to generalised curvilinear coordinates

The use of continuous mappings and generalised curvilinear coordinates is advantageous to mimic the natural material structure of the atmosphere and oceans [50]. Furthermore, soundproof models formulated in time-dependent coordinates [27, 38, 45] have much in common with compressible solvers [19]. Thus, the subsequent discussion alludes to time-dependent coordinates, even though this capability is not explicitly used in this paper.

In this generalised time-dependent curvilinear coordinate description, (3) naturally takes the compressible form, cf. with (13),

$$\frac{\partial \mathcal{G} \varrho}{\partial t} + \nabla \cdot (\mathcal{G} \varrho \mathbf{v}) = 0, \quad (16)$$

regardless of the definition of  $\varrho$  in (4). In (16),  $(\mathbf{x}, t)$  already refers to coordinates of the generalised frame — cf. with (13) — where  $\mathcal{G}(\mathbf{x}, t)$  denotes the Jacobian; although mathematical details of differential geometry are unimportant in this paper, we recall for completeness that  $\mathcal{G}^2$  is the determinant of the metric tensor that defines the fundamental metric in a space of interest where the problem is posed and solved [27]. As in section 2.1,  $\nabla \cdot \dots$  denotes the scalar product of partial derivatives with a vector, so  $d/dt = \partial/\partial t + \mathbf{v} \cdot \nabla$ , with contravariant velocity  $\mathbf{v} = \dot{\mathbf{x}}$  not necessarily equal to  $\mathbf{u}$ . The compressible form of (16) can result from either variability of coordinates in time, compressibility per se, or both.<sup>1</sup> The corresponding extension of (11) and (12) to a common symbolic form for a specific variable  $\psi$  is

$$\frac{\partial \mathcal{G} \varrho \psi}{\partial t} + \nabla \cdot (\mathcal{G} \varrho \mathbf{v} \psi) = \mathcal{G} \varrho R, \quad (17)$$

<sup>1</sup>Vice versa, an incompressible form of the continuity equation may result in a compressible system with suitable variability of coordinates in time; e.g.,  $\mathcal{G} \varrho = \text{const.}$ , as for mass based coordinates commonly used in meteorology.

with some modifications of the right-hand-sides.<sup>2</sup> Importantly, the generalised mass continuity equation (16) is a special case of (17), with predetermined  $\psi \equiv 1$  and  $R \equiv 0$  for all  $(\mathbf{x}, t)$  and equation sets. This makes the mass continuity distinct from conservation laws for specific dependent variables  $\psi$ , with a primordial role for the design of the unified integration framework of soundproof and compressible systems of PDEs, detailed in the next section.

### 3 Integration schemes

#### 3.1 Non-oscillatory forward-in-time approach

The term “non-oscillatory forward-in-time” (hereafter NFT) labels a class of second-order-accurate two-time-level algorithms built on nonlinear advection schemes that suppress/reduce/control numerical oscillations characteristic of higher-order linear schemes. An instructive archetype problem to consider is an inhomogeneous generalized advection problem for an arbitrary scalar variable  $\Psi$ ,

$$\frac{\partial G\Psi}{\partial t} + \nabla \cdot (\mathbf{V}\Psi) = G\mathcal{R} . \quad (18)$$

where vector field  $\mathbf{V}$  and scalar coefficients  $G$  and  $\mathcal{R}$  are assumed to be known functions of time and space. Although (18) is reminiscent of (16) and (17), it matches neither of them exactly; this will be addressed shortly. A forward-in-time discretisation of (18) with respect to  $\Psi$  is assumed as

$$\frac{G^{n+1}\Psi^{n+1} - G^n\Psi^n}{\delta t} + \nabla \cdot (\mathbf{V}^{n+1/2}\Psi^n) = (G\mathcal{R})^{n+1/2} , \quad (19)$$

where  $n$  and  $n + 1$  index the levels of a uniform temporal grid  $t^{n+1} = t^n + \delta t$ , and  $n + 1/2$  refers to  $O(\delta t^2)$  estimates at an intermediate time level. Standard truncation-error analysis — i.e., expanding all terms in the second-order Taylor series about  $t^n$  and representing second-order temporal partial derivatives in terms of the spatial derivatives based on the structure of the governing equation (18) [24, 36, 40] — leads to the modified equation that is approximated by (19) to  $O(\delta t)^2$ :

$$\frac{\partial G\Psi}{\partial t} + \nabla \cdot (\mathbf{V}\Psi) = G\mathcal{R} - \frac{\delta t}{2} \nabla \cdot (\mathbf{V}^*\Psi) + \frac{\delta t}{2} \nabla \cdot (\mathbf{V}\mathcal{R}) + O(\delta t^2) , \quad (20)$$

where a bogus vector field  $\mathbf{V}^*$  can be represented — cf. section 3.2.4 in [36] for a discussion — as

$$\mathbf{V}^* = \frac{1}{2} \delta t G^{-1} \left[ \mathbf{V} \left( \mathbf{V} \cdot \frac{\nabla |\Psi|}{|\Psi|} \right) + \left( \frac{\partial G}{\partial t} + \nabla \cdot \mathbf{V} \right) \mathbf{V} \right] . \quad (21)$$

The modified equation (20), including (21), reveals the functional form of the  $O(\delta t)$  error due to the uncentred-in-time differencing of  $\Psi$  in (19). Notably, the  $O(\delta t)^2$  estimates of the vector field  $\mathbf{V}$  and the rhs forcing  $G\mathcal{R}$  at the intermediate time level are sufficient to eliminate from (20) the  $O(\delta t)$  truncation errors proportional to their temporal derivatives [36].

To achieve a fully second-order-accurate forward-in-time (FT) algorithm, (19) is supplied on the rhs with explicit, at least first-order accurate, discrete representations of the negative of the error, thus compensating the error to at least  $O(\delta t)^2$ . The second term on the rhs of (20) is quadratic in  $\mathbf{V}$  and does not depend on  $\mathcal{R}$ . Its compensation is within the realm of multidimensional FT flux-form advection schemes, with linear compensations leading to schemes that can be loosely thought of as generalisations of the classical one-step Lax-Wendroff advection scheme [10, 32]. All developments reported in this paper rely on the nonlinear “multidimensional positive definite advection transport algorithm” (MP-DATA), whose underlying idea is an iterative application of the generic upwind scheme, with the initial

<sup>2</sup>For instance,  $\nabla\varphi$  in the momentum equation is replaced with the product of a coefficient matrix and the vector of partial derivatives,  $\bar{\mathbf{G}}\nabla\varphi$ , and  $\mathbf{u}$  on the rhs of the perturbation form of the  $\theta$  equation is replaced by yet another form; see Eq. (25).

iteration producing a first-order-accurate solution and subsequent iterations compensating for the errors of the preceding iterations using the negative of the bogus vector field highlighted in (21).<sup>3</sup>

The third term on the rhs of (20) couples the advection and forcing. Its compensation is technically simple and merely requires a proper implementation of the rhs forcing [35]. Consider a second-order accurate NFT advection scheme for the homogeneous case ( $\mathcal{R} \equiv 0$ ) of (18):

$$\begin{aligned}\Psi_{\mathbf{i}}^{n+1} &= \frac{G_{\mathbf{i}}^n}{G_{\mathbf{i}}^{n+1}} \left( \Psi_{\mathbf{i}}^n - \frac{\delta t}{G_{\mathbf{i}}^n} \nabla \cdot \overline{(\mathbf{V}\Psi)^{n+1/2}} d\tau \right) + \mathcal{O}(\delta t)^3 \\ &\equiv \mathcal{A}_{\mathbf{i}} \left( \Psi^n, \mathbf{V}^{n+1/2}, G^n, G^{n+1} \right),\end{aligned}\quad (22)$$

where a vector index  $\mathbf{i} = (i_1, i_2, i_3)$  marks the point  $\mathbf{x}_{\mathbf{i}}$  of a co-located grid. The first term on the rhs of the equality in (22) encapsulates the FT Taylor-series derivation procedure by expressing its outcome as a centered-in-time integral of the homogeneous (18), symbolised with an overline atop the advective flux. The identity that follows defines the MPDATA advection operator in terms of its entries. Given (22), a second-order-accurate solution to the inhomogeneous (18) can be generated as

$$\Psi_{\mathbf{i}}^{n+1} = \mathcal{A}_{\mathbf{i}} \left( \widetilde{\Psi}^n, \mathbf{V}^{n+1/2}, G^n, G^{n+1} \right) + 0.5\delta t \mathcal{R}_{\mathbf{i}}^{n+1}, \quad (23)$$

where

$$\widetilde{\Psi}^n \equiv \Psi^n + 0.5\delta t \mathcal{R}^n. \quad (24)$$

Transporting the auxiliary field  $\widetilde{\Psi}^n$  (as opposed to  $\Psi^n$ ) — i.e. using in (19)  $(G\mathcal{R})^{n+1/2} = 0.5(G\mathcal{R})^n + 0.5(G\mathcal{R})^{n+1} + \mathcal{O}(\delta t^2)$ , and incorporating  $0.5(G\mathcal{R})^n$  in the advective operator  $\mathcal{A}$  — compensates the second error term on the rhs of (20) [35].

Depending on the definitions of  $G$ ,  $\Psi$ ,  $\mathbf{V}$  and  $\mathcal{R}$ , the outlined archetype PDE (18) and its NFT integrator (23) account for problems like (17) formulated in terms of specific dependent variables as well as for problems formulated in terms of dependent variables expressed per unit of volume, the simplest example of which is (16). In the former case, typical of the soundproof models, the density  $\varrho$  is absorbed in  $G \equiv \mathcal{G}\varrho$ , whereas  $\Psi \equiv \psi$  and  $\mathcal{R} \equiv R$ . In the latter case, typical of gas dynamics, the density is absorbed in  $\Psi \equiv \varrho\psi$ , whereas  $G \equiv \mathcal{G}$  and  $\mathcal{R} \equiv \varrho R$ . In both cases  $\mathbf{V} \equiv G\mathbf{v}$ , in consequence of which  $\mathbf{V} \equiv \mathcal{G}\varrho\mathbf{v}$  or  $\mathbf{V} \equiv \mathcal{G}\mathbf{v}$ , respectively for  $\Psi$  defined as a specific or a density type variable. This duality of the interpretation benefits the efficacy of forward-in-time solvers. For example, in soundproof systems it suffices to cancel first-order truncation errors depending on the flow divergence, regardless of the complexity of the accompanying mass continuity equation. In compressible systems it enables consistency of advective transport for all dependent variables [35, 30]. These properties are important for suppressing spurious tendencies of specific variables wherever these variables are locally constant. On the other hand, the distinction between the two NFT integrators undermines numerically a consistent local comparability of soundproof and compressible solutions [20] — due to the differences in limiting the transportive momenta  $\mathcal{G}\varrho\mathbf{v}$  versus the transportive velocities  $\mathcal{G}\mathbf{v}$  [34, 30] to suppress spurious oscillations where flow features are poorly resolved. From the perspective of large-time-step semi-implicit schemes for compressible Euler equations of atmospheric dynamics, the compressible MPDATA integrators in (23) — see [35, 30, 42, 48] for examples — are nonetheless inconvenient, because of the inherent nonlinearity of the gas dynamics conservation laws, eventually leading to complex nonlinear elliptic problems. This contrasts with soundproof systems, where the corresponding NFT integrator (23) naturally lends itself to implicit representations of the rhs [28].

<sup>3</sup>The MPDATA has been developed over the three decades; see [36, 40] for comprehensive reviews or [19, 47] concise summaries. MPDATA schemes admit options extending basic second-order-accurate sign-preserving scheme to full monotonicity preservation, third-order accuracy, and variable-sign fields, and they offer numerous advantages, including nonlinear stability, robustness, physical realisability, and massively-parallel scalability [28, 25]; all calculations reported here use the monotone “infinite-gauge” variant of MPDATA, cf. section 5.1 in [39].

### 3.2 Unified NFT framework for soundproof and compressible models

Extending the soundproof NFT integrators to compressible equations, reduces to two key modifications: (i) utilise the compressible mass continuity equation in (16), together with the compressible case of the integrator in (22), not only to prognose the density but also to define the transportive momenta for all specific variables; and (ii) extend the generalised Poisson solver of the soundproof models to Helmholtz problems arising due to the constitutive law (9) and numerical formulation of the soundproof integrator in (23). The modification (i) is important for minimising numerical and programming departures between the soundproof and the compressible model, and it suffices for compressible integrations with acoustic time steps; i.e., limited by the CFL condition based on the speed of sound. The modification (ii) is essential to enable integrating compressible equations with larger time steps. The two modifications together lead to a class of conservative compressible NFT schemes with mass continuity equation integrated in the spirit of gas dynamics [42], but with the entropy and momentum equations integrated in the spirit of soundproof equations posed in time dependent geometry [19]. In the following paragraph we shall specify (i), and expose its workings in the subsequent paragraph 3.2.2 in the context of a compressible algorithm that is explicit with respect to acoustic modes and implicit with respect to buoyant and rotational modes. This unusual scheme (hereafter an “acoustic” scheme) is a derivative of the proven NFT integrator for the soundproof equations [28] and prepares the grounds for large-time-step semi-implicit integrators. The (ii) and incorporation of the resulting Helmholtz solvers into the acoustic scheme will be discussed in paragraph 3.2.3.

#### 3.2.1 Transportive momenta for specific variables in compressible flows

Standardly, the transportive momenta and advective velocities  $\mathbf{V}^{n+1/2}$  that enter (22) and (23) are evaluated either by the linear extrapolation from  $n - 1$  and  $n$  time levels, which requires storing an additional vector field, or by solving the full equation of motion to the first order [36]. The first choice is preferred for soundproof models [33], as it assures that the advective momenta satisfy mass continuity by design. The second choice circumvents the necessity of storing an extra vector field, and benefits the stability of elastic systems (e.g., compressible, shallow-water, isentropic/isopycnic models) [35]. Here we consider an alternative for compressible NFT integrators. First, the continuity equation (16) is solved by the algorithm (22), with  $\mathbf{V}^{n+1/2}$  obtained by either the linear or the nonlinear extrapolation as mentioned above. All subsequently integrated governing PDEs are viewed as (17) in terms of specific variables  $\psi$ , and employ the soundproof variant of (23), with transportive momenta  $\mathbf{V}^{n+1/2} = \overline{(\mathcal{G}\rho\mathbf{v})}^{n+1/2}$  then defined as the cumulative advective mass fluxes over MPDATA iterations taken from the preceding execution of (22) for (16); see [47] for technical exposition.

Noteworthy, the concept of advecting specific variables with mass fluxes has a long tradition in computational fluid dynamics. In flux-form anelastic models it arises naturally [6, 33] as a byproduct of an exact-projection formulation of the elliptic pressure equation that follows the anelastic mass-continuity constraint. In elastic systems it assures compatibility of finite-volume advection with Lagrangian transport of specific variables [21, 5, 16] and facilitates extensions of compressible schemes to the soundproof regime [15, 31, 16]. Here it is used complementarily to facilitate a bespoke extension of an established soundproof solver [28] to compressible Euler equations of all-scale atmospheric dynamics.

#### 3.2.2 A semi-implicit acoustic scheme

As an introduction to semi-implicit schemes for large-time-step integrations of compressible Euler equations, consider a semi-implicit algorithm for integrating the compressible equations with explicit representation of acoustic modes in (1)-(3), cast in stationary curvilinear coordinates (e.g., to accommodate

surface orography):

$$\begin{aligned}
 \frac{\partial \mathcal{G}\varrho}{\partial t} + \nabla \cdot (\mathcal{G}\varrho \mathbf{v}) &= 0, \\
 \frac{\partial \mathcal{G}\varrho \theta'}{\partial t} + \nabla \cdot (\mathcal{G}\varrho \theta' \mathbf{v}) &= -\mathcal{G}\varrho \tilde{\mathbf{G}}^T \mathbf{u} \cdot \nabla \theta_e, \\
 \frac{\partial \mathcal{G}\varrho \mathbf{u}}{\partial t} + \nabla \cdot (\mathcal{G}\varrho \mathbf{v} \otimes \mathbf{u}) &= \\
 -\mathcal{G}\varrho \left( \Theta \tilde{\mathbf{G}} \nabla \varphi + \mathbf{g} \Upsilon_B \frac{\theta'}{\theta_b} + \mathbf{f} \times (\mathbf{u} - \Upsilon_C \mathbf{u}_e) - \mathcal{M}'(\mathbf{u}, \mathbf{u}, \Upsilon_C) \right).
 \end{aligned} \tag{25}$$

Here, the notation combines those of sections 2.1 and 2.3, while incorporating further symbolism of time-dependent geometry with  $\mathbf{v} = \tilde{\mathbf{G}}^T \mathbf{u}$  and  $\tilde{\mathbf{G}}$  denoting the matrix of known metric coefficients [27, 45]. The term  $\mathcal{M}'(\mathbf{u}, \mathbf{u}, \Upsilon_C) = \mathcal{M}(\mathbf{u}, \mathbf{u}) - \mathcal{M}(\mathbf{u}_e, \mathbf{u}_e)$  symbolises metric forcings in the spherical domain; see Appendix A of [45].

In the system (25) only the mass continuity equation is homogeneous, whereas the entropy and momentum equations have nonvanishing right-hand-sides, dependent on the prognosed model variables. In consequence, the entire model algorithm reduces to two distinct steps. In the first step the density becomes updated, while constructing the transportive momenta required for the subsequent update of specific variables of potential temperature and velocity components:

$$\varrho_i^{n+1} = \mathcal{A}_i \left( \varrho^n, (\mathcal{G}\mathbf{v})^{n+1/2}, \mathcal{G}, \mathcal{G} \right) \implies \mathbf{V}^{n+1/2} = \overline{(\mathcal{G}\varrho \mathbf{v})}^{n+1/2}. \tag{26}$$

In the second step, to account for the nonlinearity of the pressure gradient force and the metric forces on the rhs of the momentum equations, the template algorithm (23) is executed iteratively lagging nonlinear terms behind:

$$\begin{aligned}
 \theta'_i{}^\nu &= \widehat{\theta}'_i - 0.5\delta t \left( \tilde{\mathbf{G}}^T \mathbf{u}^\nu \cdot \nabla \theta_e \right)_i \\
 \mathbf{u}_i^\nu &= \widehat{\mathbf{u}}_i - 0.5\delta t \left( \Theta^{\nu-1} \tilde{\mathbf{G}} \nabla \varphi^\nu + \mathbf{g} \Upsilon_B \frac{\theta'^\nu}{\theta_b} \right)_i \\
 &\quad - 0.5\delta t \left( \mathbf{f} \times (\mathbf{u}^\nu - \Upsilon_C^{\nu-1} \mathbf{u}_e) - \mathcal{M}'(\mathbf{u}, \mathbf{u}, \Upsilon_C)^{\nu-1} \right)_i,
 \end{aligned} \tag{27}$$

where  $\widehat{\theta}'_i$  and  $\widehat{\mathbf{u}}_i$  are the shorthands for the respective actions of the transport operator  $\mathcal{A}$  on  $\tilde{\theta}'$  and  $\tilde{\mathbf{u}}$  in (23)-(24):

$$\begin{aligned}
 \widehat{\theta}'_i &= \mathcal{A}_i \left( \tilde{\theta}', \mathbf{V}^{n+1/2}, \varrho^{*n}, \varrho^{*n+1} \right) \\
 \widehat{\mathbf{u}}_i &= \mathcal{A}_i \left( \tilde{\mathbf{u}}, \mathbf{V}^{n+1/2}, \varrho^{*n}, \varrho^{*n+1} \right),
 \end{aligned} \tag{28}$$

with  $\mathbf{V}^{n+1/2}$  provided by (26), and the effective densities  $\varrho^{*n}$  and  $\varrho^{*n+1}$  defined, respectively, as  $\varrho^{*n} := \mathcal{G}\varrho^n$  and  $\varrho^{*n+1} := \mathcal{G}\varrho^{n+1}$ . Furthermore,

$$\varphi_i^\nu = c_p \theta_0 \left[ \left( \frac{R_d}{p_0} \varrho^{n+1} \theta^{\nu-1} \right)^{R_d/c_p} - \pi_e \right]_i, \tag{29}$$

$$\theta_i^\nu = \left( \widehat{\theta}' - 0.5\delta t \tilde{\mathbf{G}}^T \mathbf{u}^\nu \cdot \nabla \theta_e + \theta_e \right)_i. \tag{30}$$

Throughout (27)-(30), the index  $\nu = 1, \dots, N_\nu$  numbers the iterations, with the first guess  $\theta_i^0 = \widehat{\theta}_i$  generated by advecting full  $\theta$ ,

$$\theta_i^0 = \mathcal{A}_i \left( \theta^n, \mathbf{V}^{n+1/2}, \varrho^{*n}, \varrho^{*n+1} \right) \tag{31}$$

and  $\mathbf{u}_i^0$  obtained by solving the advective form of the momentum equation to the first order [35]. With this design, the solution is fully second order accurate even for  $N_\nu = 1$ , and  $N_\nu = 2$  gives already close approximation to the trapezoidal integral.

The scheme outlined in (27)-(30) contains fully implicit trapezoidal integrals of buoyancy and Coriolis terms; whereas pressure perturbations (viz. acoustic modes), metric forcings, and coefficients depending on full potential temperature are integrated explicitly. To derive the closed-form expression for the velocity update, we substitute the potential temperature perturbation in the buoyancy term of the momentum equation with the rhs of the entropy scheme and gather all terms depending on  $\mathbf{u}^\nu$  on the lhs of the momentum scheme, while dropping the spatial grid index  $\mathbf{i}$  everywhere, as all dependent variables, coefficients and terms are co-located in (27)-(30). This results in

$$\begin{aligned} \mathbf{u}^\nu + 0.5\delta t \mathbf{f} \times \mathbf{u}^\nu &= (0.5\delta t)^2 \mathbf{g} \Upsilon_B \frac{1}{\theta_b} \widetilde{\mathbf{G}}^T \mathbf{u}^\nu \cdot \nabla \theta_e = \widehat{\mathbf{u}} - 0.5\delta t \Theta^{\nu-1} \widetilde{\mathbf{G}} \nabla \varphi^\nu \\ &= 0.5\delta t \left( \mathbf{g} \Upsilon_B \frac{\widehat{\theta}^\nu}{\theta_b} - \mathbf{f} \times \Upsilon_C^{\nu-1} \mathbf{u}_e - \mathcal{M}'(\mathbf{u}, \mathbf{u}, \Upsilon_C)^{\nu-1} \right). \end{aligned} \quad (32)$$

Viewing the lhs of (32) as a linear operator acting on the velocity vector,  $\mathbf{L}\mathbf{u}^\nu$ , (32) can be written compactly as

$$\mathbf{L}\mathbf{u}^\nu = \widehat{\mathbf{u}} - 0.5\delta t \Theta^{\nu-1} \widetilde{\mathbf{G}} \nabla \varphi^\nu, \quad (33)$$

where  $\widehat{\mathbf{u}}$  subsumes the two explicit terms on the rhs of (32). The compact expressions in (33) symbolises a system of three linear algebraic equations with three unknown components of the velocity vector  $\mathbf{u}^\nu$  at each point of the co-located grid. Consequently, the closed-form expression for the velocity update may be then symbolised as

$$\mathbf{u}^\nu = \check{\mathbf{u}} - \mathbf{C} \nabla \varphi^\nu, \quad (34)$$

where  $\check{\mathbf{u}} = \mathbf{L}^{-1} \widehat{\mathbf{u}}$ , and  $\mathbf{C} = \mathbf{L}^{-1} 0.5\delta t \Theta^{\nu-1} \widetilde{\mathbf{G}}$  denotes a  $3 \times 3$  matrix of known coefficients; cf. [27] and [44, 46] for expanded expressions in tensorial and explicit component notations. In each iteration  $\nu$  the velocity update in (34) uses the thermodynamic pressure in (29), and the total potential temperature gets updated according to (30). However, the potential temperature perturbation is updated, according to the first equation of the system (27), only upon the completion of the velocity update for  $\nu = N_\nu$ .

The acoustic scheme given above originated from an adaptation of the soundproof pseudo-incompressible algorithm [41, 44], as an extension of the anelastic algorithm [28]. In essence, it replaces a soundproof density and elliptic pressure (perturbation) with the prognosed thermodynamic density and pressure. Thus it minimises numerical differences between soundproof and compressible algorithms, and provides the reference solution for large-time-step compressible schemes for atmospheric flows. Furthermore, it represents a minimal programming effort to extend the existing soundproof modelling framework to compressible all-scale flows. Finally, this acoustic scheme forms the foundation of the semi-implicit compressible models with large time steps discussed next.

### 3.2.3 Helmholtz solvers for semi-implicit compressible models

A common feature of the anelastic and pseudo-incompressible equations in the generalised system of conservation laws (11)-(13), and thus in (16)-(17), is that the density is prescribed. This obviates the solution of the prognostic mass continuity equation and reduces the first step (26) of the unified framework to a soundproof predictor (e.g., the linear extrapolation from  $t^{n-1}$  and  $t^n$ ) of  $\mathbf{V}^{n+1/2}$  for the use in (23). Furthermore, with the density prescribed, (10) takes in stationary curvilinear coordinates a compact form

$$\nabla \cdot (\varrho^* \mathbf{v}) = 0. \quad (35)$$

Because  $\mathbf{v} = \widetilde{\mathbf{G}}^T \mathbf{u}$ , acting with  $\widetilde{\mathbf{G}}^T$  on both sides of (34), multiplying the resulting equation by  $\varrho^*$ , acting on it with  $\nabla \cdot$  and multiplying the result by  $-\delta t / \varrho^*$ , (35) produces

$$0 = -\frac{\delta t}{\varrho^*} \nabla \cdot (\varrho^* \mathbf{v}^\nu) = -\frac{\delta t}{\varrho^*} \nabla \cdot \left[ \varrho^* \left( \check{\mathbf{v}} - \widetilde{\mathbf{G}}^T \mathbf{C} \nabla \varphi^\nu \right) \right], \quad (36)$$

a (diagonally preconditioned) elliptic Poisson problem for pressure perturbation  $\varphi^\nu$ , the solution of which depends on the explicit part

$$\check{\mathbf{v}} = \widetilde{\mathbf{G}}^T \check{\mathbf{u}} \quad (37)$$

and the boundary conditions imposed on the normal component  $\mathbf{n} \cdot \mathbf{v}^\nu$  [46, 44, 27]. In soundproof models, (36) replaces the thermodynamic pressure perturbation of (29), with all other steps of the procedure (27)-(34) remaining the same. Because the soundproof models do not support acoustic modes by design, the stability of the semi-implicit scheme is controlled solely by the advective CFL. The latter is a desirable feature in simulation of low Mach number flows.

Generally, soundproof models are carefully derived to assure that they possess conservation principles, energy invariants in particular, and that their solutions converge asymptotically to respective compressible solutions [22, 23, 11, 12, 3, 8]. Consequently, their forms, coefficients and reference profiles are predetermined analytically providing a strict guidance for numerical designs. In contrast, designing large-time-step semi-implicit schemes for integrating compressible Euler equations admits substantial degree of freedom, as the primary guiding principles is the numerical efficacy of the resulting schemes. In designing our variants of large-time-step compressible schemes we adopt a premiss that the ultimate cause for acoustic schemes becoming unstable, when violating their sound-speed based CFL, is an uncontrolled growth of truncation errors in determining pressure gradient force, cf. [47] for discussion. Thus, we seek a procedure compensating for such errors while maintaining the consistency between analytic equations and the numerical formulation.

Considering the compressible case of Cartesian equations (1)-(3) and combining (9) and (3) while assuming adiabatic inviscid flows results in

$$\frac{d\pi}{dt} = -\gamma\pi\nabla \cdot \mathbf{u} \implies \frac{\partial \rho\pi}{\partial t} + \nabla \cdot (\rho\pi\mathbf{u}) = -\gamma\rho\pi\nabla \cdot \mathbf{u} \quad (38)$$

where  $\gamma \equiv R_d/c_v$ . In the adopted stationary curvilinear framework, (38) takes the form

$$\frac{\partial \varrho^* \pi}{\partial t} + \nabla \cdot (\varrho^* \mathbf{v}\pi) = -\gamma\varrho^* \pi \frac{1}{\mathcal{G}} \nabla \cdot (\mathcal{G}\mathbf{v}) . \quad (39)$$

This equation is already of the form (17), and we integrate it using a first-order-accurate variant of the NFT template algorithm (23)

$$\begin{aligned} \pi^{n+1} &= \widehat{\pi} - \delta t \gamma \pi^{n+1} \frac{1}{\mathcal{G}} \nabla \cdot (\mathcal{G}\mathbf{v}^{n+1}) + \mathcal{O}(\delta t^2), \\ \widehat{\pi} &= \mathcal{A}(\pi^n, \mathbf{V}^{n+1/2}, \varrho^{*n}, \varrho^{*n+1}) \end{aligned} \quad (40)$$

Here, the grid position index  $\mathbf{i}$  has been dropped as there is no ambiguity. Except for  $\pi^n$  all remaining arguments of the transport operator are the same as defined in (28). Integrating (39) to the first order suffices for the second-order accuracy of the entire model solution, because pressure perturbations enter the momentum equations with the factor  $0.5\delta t$ . Multiplying (40) by the constant  $c_p\theta_0$ , representing  $\pi^{n+1}$  as a sum of the perturbation and the ambient state, expanding  $\mathbf{v}^{n+1}$  as a sum of the explicit part of the solution and the pressure gradient force, cf. (36)-(37), and collecting all terms on the rhs, leads to the elliptic Helmholtz problem

$$0 = -\frac{\delta t}{\mathcal{G}} \nabla \cdot \left[ \mathcal{G} \left( \check{\mathbf{v}} - \widetilde{\mathbf{G}}^T \mathbf{C} \nabla \varphi^\nu \right) \right] - \beta(\varphi^\nu - \varphi^\dagger), \quad (41)$$

where  $\beta \equiv [\gamma(\varphi^{\nu-1} + c_p\theta_0\pi_e)]^{-1}$ ,  $\varphi^\dagger \equiv c_p\theta_0(\widehat{\pi} - \pi_e)$  with  $\widehat{\pi}$  denoting the first term on the rhs of (40), and the first guess  $\varphi^0 = \varphi^n$  taken for  $\varphi^{\nu-1}$ . Replacing the explicit thermodynamic pressure perturbations of (29) with (41), while retaining all other elements of the a semi-implicit acoustic scheme the same, leads to semi-implicit compressible solver stable for large time steps that are comparable to those admitted

in the soundproof models. Notably, (41) requires only minor changes to adapt the variational Krylov subspace solver designed for the Poisson problem (36).

Numerical experimentation with the global baroclinic instability benchmark revealed that the large-time-step semi-implicit model actually admits time steps only half of the soundproof models. Closer examination of the derived Helmholtz problem (hereafter referred to as “first kind”) reveals that advecting the full Exner pressure in (40) adds an explicit term to the vertical velocity update that is proportional to the vertical counterpart of  $\mathbf{v}^{n+1/2} \cdot \nabla \pi_e$ , proportional itself to  $g/\theta_e$  and arguably degrading the stability of the semi-implicit representation of buoyant motions. To verify and mitigate this aspect, and to concomitantly illustrate the degree of freedom available in developing large-time step semi-implicit schemes for compressible flows, a variant of the Helmholtz problem can be designed (hereafter “second kind”) by formulating (38) in the perturbational form, in analogy to the entropy equation (2) that leads to implicit treatment of buoyancy forces in the soundproof case,

$$\begin{aligned} \frac{d\pi'}{dt} &= -\gamma\pi\nabla \cdot \mathbf{u} - \mathbf{u} \cdot \nabla \pi_e \quad \Rightarrow \\ \frac{\partial \rho \pi'}{\partial t} + \nabla \cdot (\rho \pi' \mathbf{u}) &= -\gamma \rho \pi \nabla \cdot \mathbf{u} - \rho \mathbf{u} \cdot \nabla \pi_e \end{aligned} \quad (42)$$

Anticipating the adaption of the Krylov Poisson solver for the resulting Helmholtz problem of the second kind, we seek a conservative formulation free of the new additional convective derivative on the rhs of (42). Rewriting the last term on the rhs of the second equation in (42) as  $\rho \mathbf{u} \cdot \nabla \pi_e = \nabla \cdot (\pi_e \rho \mathbf{u}) - \pi_e \nabla \cdot (\rho \mathbf{u})$ , expressing the result in the curvilinear coordinates and manipulating terms, we arrive at

$$\frac{\partial \varrho^* \pi'}{\partial t} + \nabla \cdot (\varrho^* \mathbf{v} \pi') = - \left[ \gamma \varrho^* \pi \frac{1}{\mathcal{G}} \nabla \cdot (\mathcal{G} \mathbf{v}) + \nabla \cdot (\varrho^* \mathbf{v} \pi_e) - \pi_e \nabla \cdot (\varrho^* \mathbf{v}) \right], \quad (43)$$

which after integrating with the NFT scheme similarly to (40) and further manipulating the terms becomes

$$0 = -\delta t \left[ \frac{1}{\mathcal{G}} \nabla \cdot (\mathcal{G} \mathbf{v}) + \frac{1}{\gamma} \frac{\pi_e}{\pi} \frac{1}{\varrho^* \pi_e} \nabla \cdot (\varrho^* \pi_e \mathbf{v}) - \frac{1}{\gamma} \frac{\pi_e}{\pi} \frac{1}{\varrho^*} \nabla \cdot (\varrho^* \mathbf{v}) \right] - \beta(\varphi - \widehat{\varphi}), \quad (44)$$

where  $\widehat{\varphi}$  denotes the action of the transport operator on  $\varphi$ . Recalling that  $\mathbf{v} = \check{\mathbf{v}} - \widetilde{\mathbf{G}}^T \mathbf{C} \nabla \varphi$ , it can be seen that the operator in the square brackets is composed of three Poisson operators like those in (36) and (41).

## 4 Results

### 4.1 Global baroclinic instability

In [29] the authors adopted the global baroclinic instability benchmark of [14] for the NFT integrations of the Lipps-Hemler anelastic nonhydrostatic equations embedded in (1)-(3). We refer the interested reader to [29] for the details of implementation, grid convergence study and a thorough discussion of the comparison with the hydrostatic primitive-equation results in [14]. Further results using anelastic and pseudo-incompressible equations with explicit and implicit representation of buoyant modes as well as flux-form Eulerian and semi-Lagrangian NFT integrators were presented in [43]; the semi-Lagrangian NFT integrators for the unified framework are highlighted in [47]. The calculations reported follow the setups of [43], with second-order numerics on a proof-of-concept coarse  $64 \times 128$  ( $2.8^\circ$ ) latitude-longitude grid and 23 km deep atmosphere resolved with 47 uniform  $\delta z$  intervals. The soundproof calculations and the semi-implicit compressible solver of the second kind use 2880 time steps  $\delta t = 300$  s, whereas the semi-implicit compressible solver of the first kind uses 5760 time steps with  $\delta t$  halved. The compressible calculations with explicit representation of acoustic modes employ 432000 times steps

$\delta t = 2$  s. The horizontal grid is distributed over the  $8 \times 16$  processor array of the IBM “Power 7” machine, with the resulting wallclock times for the 10 day integrations 2.1, 2.3, 3.7, 2.0, and 178.9 min, respectively, for the anelastic, pseudo-incompressible, semi-implicit compressible solvers of the first and the second kind, and the acoustic calculations. The corresponding wallclock times per time step are: 0.044, 0.048, 0.039, 0.041, and 0.025 s.

Figure 1 displays instantaneous surface potential temperature perturbations about the ambient equilibrium for the conservative NFT solutions of fully compressible Euler equations, integrated with the semi-implicit large-time-step solvers of the second and the first kind and the acoustic reference algorithm of section 3.2.2. The differences between the three results are negligible, which is not surprising as the time scale of the global baroclinic instability development (days) is well resolved with both large time steps (300 and 150 s) and acoustic (2 s)  $\delta t$ . To assess solution correspondence of the compressible and soundproof equations, Fig. 2 displays the large-time step  $\delta t = 300$  s results for the compressible, pseudo-incompressible, and anelastic PDEs. While the compressible and pseudo-incompressible solutions agree reasonably well, the anelastic result (displayed with half of the contour interval) evinces an about twice smaller amplitude of the perturbations and of the maximal wind. The corresponding semi-Lagrangian experiments (not shown) corroborate this relative disparity between the anelastic and the pseudo-incompressible or compressible simulations, even though the amplitude of all semi-Lagrangian results is about 20% smaller than of the corresponding conservative Eulerian results. Furthermore, juxtaposing Figs. 1 and 2 reveals that while all compressible calculations agree closely both in amplitude and phase, the propagation of baroclinic eddies is the slowest in the compressible runs, faster for the pseudo-incompressible case and the fastest (at about  $1 \text{ m s}^{-1}$  compared to the compressible solutions) for the anelastic case.

The suitability of soundproof models for weather and climate prediction has been questioned on the grounds of normal-mode analysis [9, 3]. The current results tend to emphasise nonlinear baroclinic vorticity production [47], hinted already in Fig. 1 evincing steeper fronts for the pseudo-incompressible and compressible results. The observed differences between the anelastic and the remaining results appear relatively insignificant in earlier linear stages of the wave development [29, 43]; and the effect is transient, as the anelastic solution also produces steep fronts by day 10 and ultimately all solutions transition to turbulent jets, Fig. 3. While such differences are significant for NWP, due to the transiency they may have little impact on numerical climate prediction, as suggested by the comparability of the soundproof and compressible simulations of the idealised Held-Suarez climate [51] or aqua planet computational studies [1].

## 4.2 Amplification and breaking of stratospheric gravity waves

The example of the preceding section addressed 3D hydrostatic dynamics even though simulated with nonhydrostatic equations. Here we consider an essentially nonhydrostatic 2D problem. A small amplitude wave packet — excited, say, by a squall line with the top impinging upon the tropopause [26] — propagates into the stratosphere. Because density of the media decreases with altitude, the amplitude of the wave increases with height in proportion to  $\rho_b^{-1/2}$ . When the wave amplitude becomes comparable with the vertical wavelength, the problem becomes inherently nonlinear. Then, the wave overturns and breaks generating bursts of turbulence far from the excitation region. The problem is numerically challenging, because it covers about nine density height scales<sup>4</sup> and vertical wavelengths, and a transition from the linear-wave regime near the bottom of the domain to a vigorous turbulent flow with a broad range of scales about 30 km aloft. It has been recently documented in [44], where the soundproof NFT solutions generated on structured grids and unstructured meshes were analysed in the context of asymptotic theory [2].

<sup>4</sup>This amounts to the four orders of magnitude density decrease over the model depth.

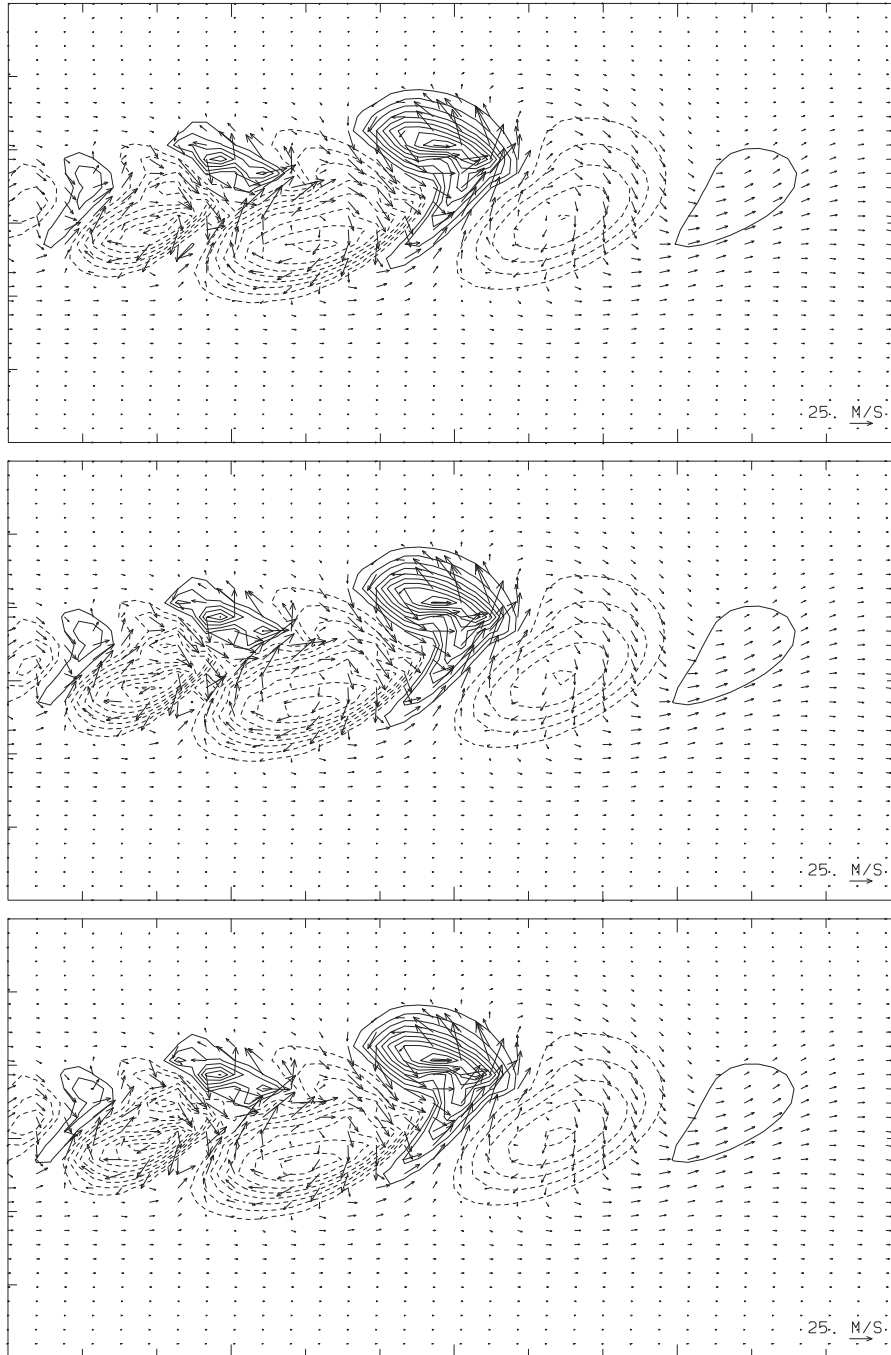


Figure 1: Baroclinic instability, day 8: surface potential temperature perturbations on the horizontal subdomain  $[90, 270] \times [0, 90]$  degrees, for compressible Euler equations integrated with the semi-implicit large-time-step algorithms of the first and second kind (top and centre, respectively) and the acoustic algorithm (bottom). Positive/negative contour values are displayed with solid/dashed lines, and zero contour lines are not shown; the contour interval is 4 K, and the corresponding maximal horizontal wind vectors are 49, 47 and 44  $\text{m s}^{-1}$ .

Following [44], the model setup assumes an isothermal stratosphere, with temperature  $T_o = 222.65$  K, and the ambient wind of constant speed  $u_e = U = 20 \text{ m s}^{-1}$ , and the ambient profile of potential temperature  $\theta_e(z) = \theta_b$ . The 60 km deep and 120 km wide model domain is resolved (in transformed computational domain using terrain-following curvilinear coordinates) with  $319 \times 159$  uniform grid

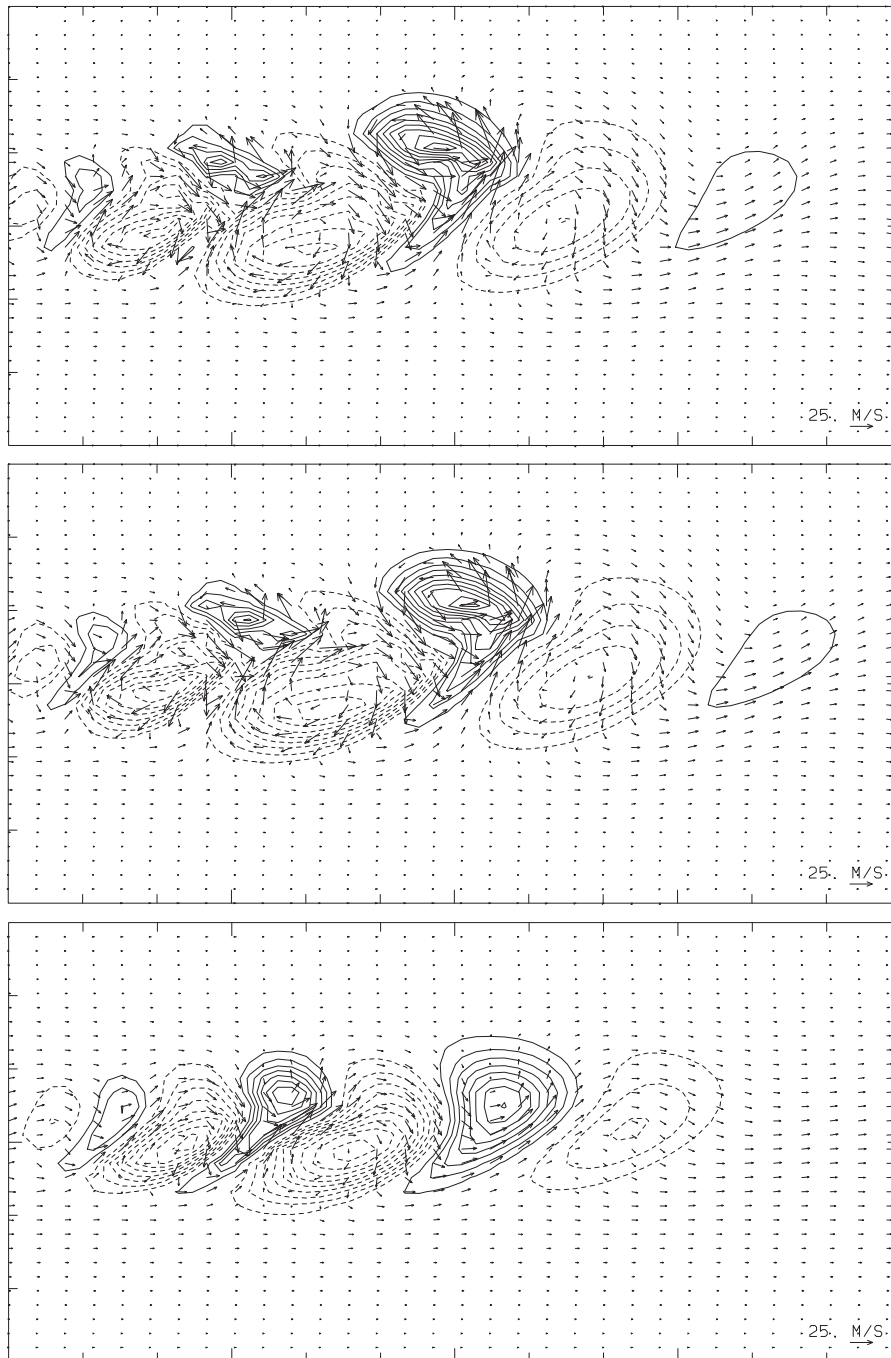


Figure 2: As Fig. 1, but comparing the  $\delta t = 300$  s large-time-step solutions for the compressible (top), pseudo-incompressible (centre) and anelastic (bottom) nonhydrostatic models. The contour interval is 2 K for the anelastic run and 4 K otherwise. The respective maximal horizontal wind vectors are 44, 50, and 29  $\text{m s}^{-1}$

intervals  $\delta x \approx \delta z \approx 380$  m. The wave is excited by a small deflection of a lower boundary embedded in the ambient flow, centred at the origin of the  $[-60, 60] \times [0, 60]$   $\text{km}^2$   $(x, z)$ -domain. The problem is inherently nonhydrostatic because the dominant horizontal wavenumber (the reciprocal of the boundary deflection half width) equals the asymptotic wavenumber  $N/U$  of the induced gravity wave; where  $N$  denotes the buoyancy frequency. Furthermore, the problem is only weakly nonlinear with respect to linear Boussinesq theory [44]. The onset of wave breaking in the upper half of the model domain is

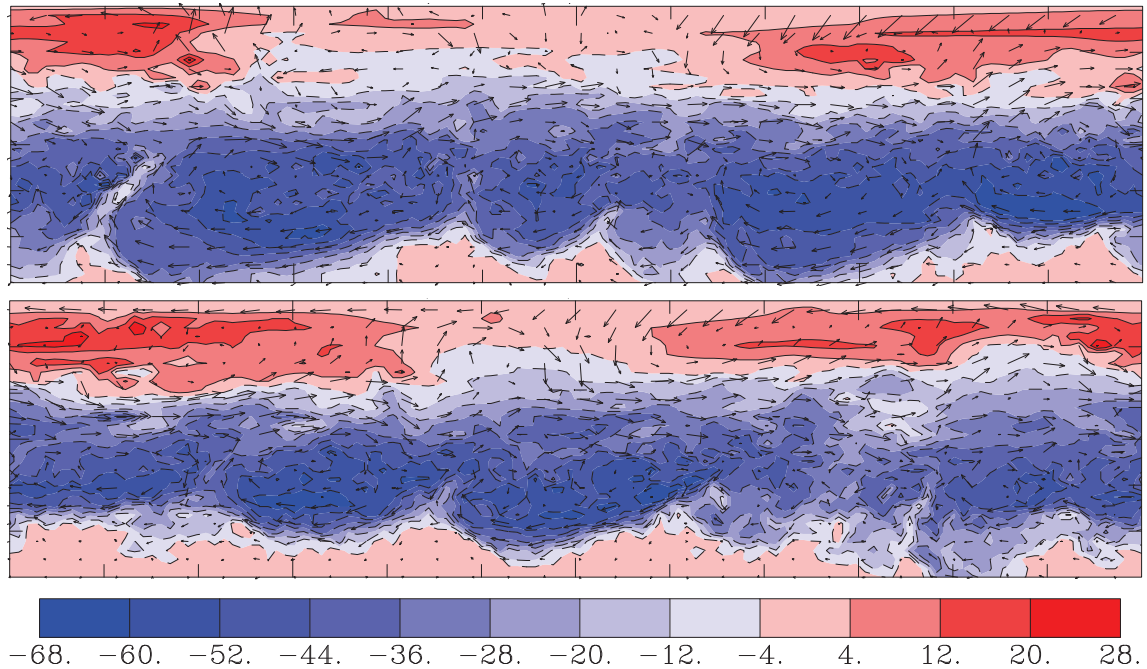


Figure 3: Baroclinic instability, day 30: surface potential temperature perturbations on the northern hemisphere's subdomain  $[0, 360] \times [0, 90]$  degrees, for compressible Euler equations integrated with the semi-implicit large-time-step algorithms of the second kind (top) and the anelastic (bottom). Maximal winds reach  $60\text{m s}^{-1}$  in both solutions.

observed after 90 min of the simulated time.

Figure 4 displays the isentropes ( $\ln \theta$ ) at the onset of breaking, simulated with the semi-implicit compressible solver (of the second kind) and the pseudo-incompressible and anelastic soundproof solvers. All large-time step calculations (including the semi-implicit compressible solver of the 1st kind; not shown) employed the soundproof time step  $\delta t = 5$  s. All calculations with soundproof  $\delta t$  were conducted on 32 cores of the IBM “Power 7” machine with insignificant (less than a minute) wall clock time. Consistent with [16, 44], the two soundproof systems produce virtually the same solution, also closely matched by the large-time step semi-implicit compressible solvers.

## 5 Remarks

A class of established non-oscillatory forward-in-time (NFT) methods for integrating soundproof equations of atmospheric dynamics [19] has been combined with the corresponding NFT solvers for gas dynamics [42], to form a unified numerical framework for integrating conservation laws of all-scale atmospheric flow problems. The foundation of the unified framework lies in assigning the dual, primordial role to the prognostic mass continuity equation: first as a prognostic thermodynamic variable, standard in gas dynamics; and second as a weighting factor shaping conservation laws for specific dependent variables (alias, mixing ratios), standard in soundproof models. In consequence of the latter, prognosis of the thermodynamic density also defines transportive momenta for subsequent advection of specific variables as cumulative directional mass fluxes. This offers several advantages for the effective prognosis of the specific variables. Given that both density and all specific variables use the same transport algorithm, advection of specific variables preserves their local constancy. Furthermore, flux-limiting of specific variables is consistent with their Lagrangian properties and synchronised naturally with the

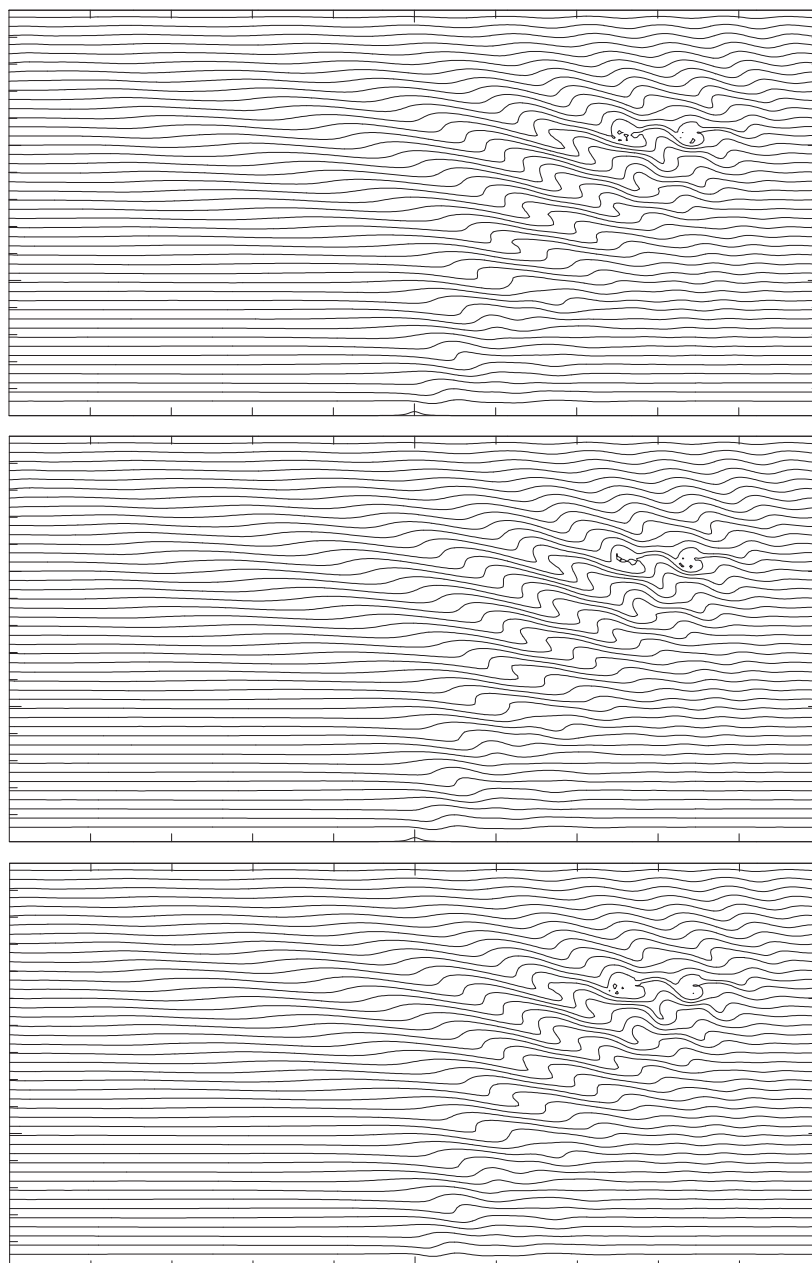


Figure 4: Isentropes ( $\ln \theta$ ) at the onset of breaking simulated with the semi-implicit compressible solver of the second kind (top), and the pseudo-incompressible and anelastic soundproof solvers (centre and bottom, respectively).

limiting of the density. Most importantly, even though conservative, the solution is directly specified in terms of specific variables, and this facilitates the design of semi-implicit solvers for compressible systems.

In computational meteorology the soundproof and compressible models are often opposed against each other as exclusive schools of thought. This study shows, however, that they are elements of a more general theoretical/numerical approach. In particular, the respective PDEs can be integrated using essentially the same numerics. This offers refined possibilities for comparing relative merits compressible

and soundproof equations (cf. [20]), and paves new ways for extending soundproof models to fully compressible PDEs. Quite likely future global atmospheric models will hybridise the strengths of various theoretical formulations (viz. equations), integration schemes and discretisation methods [18, 4]. The common framework capable of accommodating all-scale compressible and soundproof fluid equations with spatial discretisation on structured grids and unstructured meshes [46] is a consequent step towards such a design.

## Acknowledgments:

This work was supported by funding received from the European Research Council under the European Union's Seventh Framework Programme (FP7/2012/ERC Grant agreement no. 320375).

## References

- [1] B.J. Abiodun, J.M. Prusa, W.J. Gutowski, Implementation of a non-hydrostatic, adaptive-grid dynamics core in CAM3. Part I: comparison of dynamics cores in aqua-planet simulations, *Clim. Dyn.* 31 (2008) 795–810.
- [2] U. Achatz, R. Klein, F. Senf (2010), Gravity waves, scale asymptotics and the pseudo-incompressible equations, *J. Fluid Mech.* 663 (2010) 120–147.
- [3] A. Arakawa, C. Konor, Unification of the anelastic and quasi-hydrostatic systems of equations, *Mon. Weather Rev.* 137 (2009), 710-726.
- [4] T. Benacchio, W.P. O'Neill, R. Klein, A blended sound-proof-to-compressible numerical model for atmospheric dynamics, *Month. Weather Rev.* (2013) submitted.
- [5] P.N. Blossey, D.R. Durran, Selective monotonicity preservation in scalar advection, *J. Comput. Phys.* 227 (2008) 5160–5183.
- [6] T.L. Clark, A small-scale dynamic model using a terrain-following coordinate transformation, *J. Comput. Phys.* 24 (1977) 186–215.
- [7] T.L. Clark, R.D. Farley, Severe downslope windstorm calculations in two and three spatial dimensions using anelastic interactive grid nesting: a possible mechanism for gustiness. *J. Atmos. Sci.* 41 (1984) 329–350.
- [8] C.J. Cotter, D.D. Holm, Variational formulations of sound-proof models, *Q.J.R. Meteorol. Soc.*, (2013) in press.
- [9] T. Davies, A. Staniforth, N. Wood, J. Thuburn, Validity of anelastic and other equation sets as inferred from normal-mode analysis. *Q.J.R. Meteorol. Soc.* 129 (2003) 2761-2775.
- [10] J.K. Dukowicz, J.D. Ramshaw, Tensor viscosity method for convection in numerical fluid dynamics, *J. Comput. Phys.* 32 (1979) 3890-3893.
- [11] D.R. Durran, Improving the anelastic approximation. *J. Atmos. Sci.* 46 (1989) 1453-1461.
- [12] D.R. Durran, A physically motivated approach for filtering acoustic waves from the equations governing compressible stratified flow, *J. Fluid Mech.* 601 (2008) 365-379.

- [13] W.W Grabowski, P.K. Smolarkiewicz, A multiscale anelastic model for meteorological research, *Month. Weather Rev.* 130 (2002) 939-956.
- [14] C. Jablonowski, D.L. Williamson, A baroclinic instability test case for atmospheric model dynamical cores, *Q.J.R. Meteorol. Soc.* 132 (2006) 2943-2975.
- [15] R. Klein, Semi-implicit extension of a Godunov-type scheme based on low Mach number asymptotics I: One-dimensional flow, *J. Comput. Phys.* 121 (1995) 213-237.
- [16] R. Klein, Asymptotics, structure, and integration of sound-proof atmospheric flow equations, *Theor. Comput. Fluid Dyn.* 23 (2009) 161-195.
- [17] R. Klein, On the regime of validity of sound-proof model equations for atmospheric flows. *Proceedings of the ECMWF Workshop on Nonhydrostatic Modelling, 8-10 November, 2010, Reading, UK*, (2011) 35-53.
- [18] C. Konor, Design of a Dynamical Core Based on the Nonhydrostatic "Unified System" of Equations. *Month. Weather Rev.* doi:10.1175/MWR-D-13-00187.1, in press.
- [19] C. Kühnlein, P.K. Smolarkiewicz, A. Dörnbrack, Modelling atmospheric flows with adaptive moving meshes, *J. Comput. Phys.* 231 (2012) 2741-2763.
- [20] M. Kurowski, W.W. Grabowski, and P.K. Smolarkiewicz, 2013: Towards multiscale simulation of moist flows with soundproof equations, *J. Atmos. Sci.* (2013) in press doi:10.1175/JAS-D-13-024.1, in press.
- [21] B. Larrouturou, How to preserve the mass fractions positivity when computing compressible multi-component flows, *J. Comput. Phys.* 95 (1991) 59-84.
- [22] F.B. Lipps, R.S. Hemler, A scale analysis of deep moist convection and some related numerical calculations, *J. Atmos. Sci.* 39 (1982) 2192–2210.
- [23] F.B. Lipps, On the anelastic approximation for deep convection, *J. Atmos. Sci.* 47 (1990) 1794-1798.
- [24] L.G. Margolin, P.K. Smolarkiewicz, Antidiffusive velocities for multipass donor cell advection, *SIAM J. Sci. Comput.* 20 (1998) 907-929.
- [25] Z.P. Piotrowski, A.A. Wyszogrodzki, P.K. Smolarkiewicz, Towards petascale simulations of atmospheric circulations with soundproof models, *Acta Geophysica* 59 (2011) 1294–1311.
- [26] J.M. Prusa, P.K. Smolarkiewicz, R.R. Garcia, Propagation and breaking at high altitudes of gravity waves excited by tropospheric forcing, *J. Atmos. Sci.* 53 (1996) 2186-2216.
- [27] J.M. Prusa, P.K. Smolarkiewicz, An all-scale anelastic model for geophysical flows: dynamic grid deformation, *J. Comput. Phys.* 190 (2003) 601-622.
- [28] J.M. Prusa, P.K. Smolarkiewicz, A.A. Wyszogrodzki, EULAG, a computational model for multi-scale flows, *Comput. Fluids* 37 (2008) 1193-1207
- [29] J.M. Prusa, W.J. Gutowski, Multi-scale features of baroclinic waves in soundproof, global simulations with EULAG, *Proc. V European Conference on Computational Fluid Dynamics*, Lisbon, Portugal, 2010, ECCOMAS paper #1453, 18 pp.
- [30] C. Schär, P.K. Smolarkiewicz, A synchronous and iterative flux-correction formalism for coupled transport equations, *J. Comput. Phys.* 128 (1996) 101-120.

- [31] T. Schneider, N. Botta, K.J. Geratz, R. Klein, Extension of finite volume compressible flow solvers to multi-dimensional, variable density zero Mach number flows, *J. Comput. Phys.*, 155 (1999) 248-286.
- [32] P.K. Smolarkiewicz, The multidimensional Crowley advection scheme, *Month. Weather Rev.* 110 (1982) 1968-1983.
- [33] P.K. Smolarkiewicz, T.L. Clark, The multidimensional positive definite advection transport algorithm: Further Development and applications, *J. Comput. Phys.* 67 (1986) 396-438.
- [34] P.K. Smolarkiewicz, W.W. Grabowski, The multidimensional positive definite advection transport algorithm: Nonoscillatory Option, *J. Comput. Phys.*, 86 (1990) 355-375.
- [35] P.K. Smolarkiewicz, L.G. Margolin, On forward-in-time differencing for fluids: Extension to a curvilinear framework, *Month. Weather Rev.* 121 (1993) 1847-1859.
- [36] P.K. Smolarkiewicz, L.G. Margolin, MPDATA: A finite-difference solver for geophysical flows, *J. Comput. Phys.* 140 (1998) 459-480.
- [37] P.K. Smolarkiewicz, L.G. Margolin, A.A. Wyszogrodzki, A class of nonhydrostatic global models, *J. Atmos. Sci.* 58 (2001) 349-364.
- [38] P.K. Smolarkiewicz, J.M. Prusa, Towards mesh adaptivity for geophysical turbulence: continuous mapping approach, *Int. J. Numer. Meth. Fluids* 47 (2005) 789-801.
- [39] P.K. Smolarkiewicz, J. Szmelter, MPDATA: An Edge-Based Unstructured-Grid Formulation, *J. Comput. Phys.* 206 (2005) 624-649.
- [40] P.K. Smolarkiewicz, Multidimensional positive definite advection transport algorithm: an overview, *Int. J. Numer. Meth. Fluids* 50 (2006) 1123-1144.
- [41] P.K. Smolarkiewicz, A. Dörnbrack, Conservative integrals of adiabatic Durran's equations. *Int. J. Numer. Meth. Fluids* 56 (2008) 1529-1534.
- [42] P.K. Smolarkiewicz, J. Szmelter, Iterated upwind schemes for gas dynamics, *J. Comput. Phys.* 228 (2009) 33-54.
- [43] P.K. Smolarkiewicz, Modeling atmospheric circulations with soundproof equations. *Proceedings of the ECMWF Workshop on Nonhydrostatic Modelling, 8-10 November, 2010, Reading, UK*, (2011) 1-15.
- [44] P.K. Smolarkiewicz, J. Szmelter, A nonhydrostatic unstructured-mesh soundproof model for simulation of internal gravity waves, *Acta Geophysica* 59 (2011) 1109-1134.
- [45] P.K. Smolarkiewicz, P. Charbonneau, EULAG, a computational model for multiscale flows: An MHD extension, *J. Comput. Phys.* 236 (2013) 608-623.
- [46] P.K. Smolarkiewicz, J. Szmelter, A.A. Wyszogrodzki, An unstructured-mesh atmospheric model for nonhydrostatic dynamics, *J. Comput. Phys.* 254 (2013) 184-199.
- [47] P.K. Smolarkiewicz, C. Kühnlein, N.P. Wedi, A unified framework for discrete integrations of soundproof and compressible PDEs of atmospheric dynamics, *J. Comput. Phys.* (2013) submitted.
- [48] J. Szmelter, P.K. Smolarkiewicz, An edge-based unstructured mesh discretisation in geospherical framework, *J. Comput. Phys.* 229 (2010) 4980-4995.
- [49] A. Warn-Varnas, J. Hawkins, P.K. Smolarkiewicz, S.A. Chin-Bing, D. King, Z. Hallock, Solitary wave effects north of Strait of Messina, *Ocean Modelling* 18 (2007) 97-121.

- [50] N.P. Wedi, P.K. Smolarkiewicz, Extending Gal-Chen and Somerville terrain-following coordinate transformation on time dependent curvilinear boundaries, *J. Comput. Phys.* 193 (2004) 1–20.
- [51] N.P. Wedi, P.K. Smolarkiewicz, 2009: A Framework for testing global nonhydrostatic models. *Q.J. Roy. Meteorol. Soc.*, 135 (2009) 469-484.
- [52] N.P. Wedi, M. Hamrud, G. Mozdzynski, G. Austad, S. Curic, J. Bidlot, Global, non-hydrostatic, convection-permitting, medium-range forecasts: progress and challenges. *ECMWF Newsletter No. 133* (2012) 17-22.